Journal of Biomedical Materials Research Part B: Applied Biomaterials

WILEY

Society For Biomaterials

RESEARCH ARTICLE OPEN ACCESS

Targeting the Glial Scar: Biomaterial and Drug-Based Strategies for Modulation In Vitro

Luise Schlotterose[1,2] | Duygu Dengiz[3] | Meryem G. Ersahin[3] | Eckhard Quandt[3] | Karsten Steffens[4] | Dennis Schade[4] | Francois Cossais[1] | Ralph Lucius[1] | Kirsten Hattermann[1]

[1]Institute of Anatomy, Kiel University, Kiel, Germany | [2]Department of Physiology, Anatomy and Genetics, University of Oxford, Oxford, UK | [3]Chair for Inorganic Functional Materials, Institute for Materials Science, Kiel University, Kiel, Germany | [4]Department of Pharmaceutical and Medicinal Chemistry, Institute of Pharmacy, Kiel University, Kiel, Germany

Correspondence: Luise Schlotterose (luise.schlotterose@dpag.ox.ac.uk)

Received: 27 August 2025 | **Revised:** 6 November 2025 | **Accepted:** 21 November 2025

Keywords: glial scar | material-cell interactions | nitinol | shape memory alloys | surface energy and roughness | transforming growth factor-β

ABSTRACT

Glial scarring creates a significant obstacle for axonal regeneration in the central nervous system after injury and represents one of the main hurdles for neural microelectrode development. In this study, we established a test system for evaluating potential therapeutics and biomaterials prior to in vivo studies. The human cell line-based in vitro model replicates key glial scar characteristics such as galectin-3 expression and extracellular matrix accumulation. Moreover, we demonstrated how the model can be used to assess and validate new drug targets to reduce glial scar formation by modulating the transforming growth factor-β receptor types I and II. Beyond drug testing, our approach integrates a broad biomaterials science perspective, combining innovative chemical fabrication techniques with a complex in vitro co-stimulation system to investigate biological responses at the cell-material interface. To exemplify this, we explored the effects of sputter-coated free-standing nitinol as an exemplary implant material, along with gold and platinum electrode surfaces with varying characteristics, on glial scar-associated gene expression. By leveraging bioinspired material strategies, this platform enables the validation of promising drug candidates and their modes of action while optimizing neural implant materials to limit glial scar formation. Ultimately, this approach accelerates the development of strategies for central nervous system regeneration.

1 | Introduction

Glial scarring poses a significant obstacle to neuronal regeneration following central nervous system (CNS) injuries, creating a physical barrier to axonal regrowth [1]. This physical barrier is primarily composed of reactive microglial cells and astrocytes [2, 3], with the reactive astrocytes forming a dense shield by develop tight junctions among each other, which is one of multiple characteristics for glial scars [4]. Furthermore, these astrocytes actively produce an extensive extracellular

Abbreviations: AFM, Atomic Force Microscopy; ALK-4,-5,-7, Activin receptor-like kinase-4,-5,-7; Ar, Argon; Au, Gold; BSA, Bovine Serum Albumin; CNS, Central nervous system; CSPGs, Chondroitin Sulfate Proteoglycans; DAPI, 4′,6-diamidino-2-phenylindole; DI, Deionized water; DLC, Diamond-Like-Carbon; DMEM, Dulbecco's modified Eagle's medium; DMSO, Dimethyl sulfoxide; DNA, Deoxyribonucleic acid; ECM, Extracellular matrix; FBS, Fetal bovine serum; GAG, Glycosaminoglycan; HUVEC, Human endothelial cells; IL-10, Interleukin-10; IL6, Interleukin 6; IrO2, Iridium; ITO, Indium tin Oxide; IV, Oxide; LPS, Lipopolysaccharide; MRI, Magnetic resonance imaging; mRNA, Messenger ribonucleic acid; NiTi, Nickel Titanium; OGD, Oxygen Glucose Deprivation; PBS, Phosphate-buffered saline; PEG400, Polyethylene Glycol 400; PFA, Paraformaldehyde; Pt, Platinum; qPCR, Quantitative polymerase chain reaction; RF, Radio Frequency; RMS, Root-mean-square; RNA, ribonucleic acid; RTA, Rapid thermal annealing; SAR, Structure–activity relationship; SCA, Static contact angle; SEM, Scanning Electron Microscopy; SiO_2, Silicon dioxide; SLM, Selective laser melted; TGFβ, Transforming growth factor beta; Ti, Titanium; TiN, Titanium nitride; TiO_2, Titanium dioxide; TβRI/II, Type I/II TGFβ receptors; WFL, *Wisteria floribunda* lectin.

Luise Schlotterose and Duygu Dengiz contributed equally to this work.

matrix (ECM) rich in proteoglycans, tenascin glycoproteins, and fibronectin, forming a dense sheet. Notably, the composition of ECM proteins can vary across different zones of the scar [5, 6]. While glial scars provide essential protective functions such as sealing lesion sites, preserving uninjured tissue, and restoring homeostasis [7], they also create a microenvironment that can contribute to neurotoxicity, resulting in axon demyelination and the death of surrounding neurons [8, 9]. Reactive astrocytes, particularly, have been identified as neurotoxic as they release saturated lipids that exacerbate neurotoxic effects [9].

In a simplified description, homeostatic astrocytes can transit to a reactive state through classical activation induced by factors such as lipopolysaccharide (LPS) or, alternatively, be triggered by cytokines such as transforming growth factor-β (TGFβ). Commonly used terms include classically activated astrocytes (A1), which are described as proinflammatory and cytotoxic. In contrast, alternatively activated astrocytes (A2) are known for their anti-inflammatory properties and exhibit neuroprotective effects [10, 11]. Moreover, A2 astrocytes play a role in tissue remodeling, wound healing, and scar formation [12].

Neural implants represent one cause of glial scars in the CNS [13, 14]. Implantable microelectrodes may potentially be integrated into neural prostheses to restore lost nerve function [15]. Currently, the most common materials used for neural implants are a combination of polymers as substrates and metal or metal composite as electrodes [e.g., gold (Au), platinum (Pt) or indium tin oxide (ITO)] [15–18]. One material among those that have been investigated in this context is nitinol (NiTi, Nickel titanium). NiTi is utilized in orthodontics, self-expanding stents, atrial occlusion devices, and ophthalmology [19], but it also has shown promising results as a biomaterial for neural implants such as nerve cuff electrodes [20] and expandable microwire electrode arrays [21]. Nevertheless, NiTi is mostly used due to its ability to show shape memory effects or superelasticity owing to the diffusionless phase transformation between the high-temperature austenite phase and the low-temperature martensite phase [22]. Here, shape can be recovered either by introducing heat or removing the load, which leads to self-expanding implants [23]. Thus, they can be deployed via a catheter to complex areas in the vascular system in a minimally invasive manner. Since NiTi has self-supporting and flexible mechanical properties, it can be used as a substrate without any polymers, minimizing tissue damage. It can be modified, for example, by sputter coating in order to accommodate electrodes [24, 25].

There are already in vitro models of glial scar formation for implant materials such as metals [26, 27] and polymers [28–31]. Especially stainless steel has been studied in the context of neural implants and previously in vitro glial scar models created by Polikov et al. [32, 33] Nevertheless, stainless steel has limitations such as corrosion in ionic biological environments that might cause toxicity [18, 34] and, due to its fragile nature, the material might fracture under micromotions that could cause implant failure. As a result, it is no longer considered a first-line material for neuroimplants [18, 35]. In contrast, the superelasticity of NiTi, which allows deformation up to 8% without permanent damage [36], overcomes these mechanical limitations. NiTi shows excellent biocompatibility, corrosion resistance, magnetic resonance imaging (MRI) compatibility, and kink resistance [16, 37–39].

Use of advanced biomaterials such as NiTi for neural implants can be highly beneficial for overcoming glial scar formation. In addition to material modifications, different interventions on cellular responses have been investigated for their ability to reduce glial scarring. Most notably in this context is the inhibition of pathways leading to glial scar formation [40]. TGFβ, in particular, is linked to fibrosis [41, 42] and has been the focus of many studies aimed at inhibiting the TGFβ pathway to prevent scar formation [43–45].

In this study, we developed an in vitro model of a glial scar based on stable human cell lines and applied different strategies to reduce glial scar formation. The model consists of TGFβ-activated astrocytes and magnetron-sputtered NiTi free-standing thin films as an example neural implant material. The NiTi free-standing thin films were further modified by sputtering with Au, using Pt as possible electrodes and silicon dioxide (SiO_2) as an insulation layer. Surface material properties such as surface roughness and energy were investigated to determine their respective effects on glial scarring. Furthermore, small-molecule inhibition of TGFβ receptor type I (TβRI) and type II (TβRII) was evaluated as a prospective drug target for reducing glial scar formation. This simplified system, combining TGFβ-activated astrocytes with magnetron-sputtered NiTi free-standing thin films, serves as an easy-to-use initial evaluation platform that can be adapted for broader biomaterial and treatment screening. By providing a reliable test system for potential therapeutics, this study will help accelerate the optimization of neural implant materials and inform future in vivo studies.

2 | Materials and Methods

2.1 | Cell Culture

The human fetal astrocyte cell line SVGA was a gift from Christine Hanssen Rinaldo, University Hospital of North Norway [46] with the permission of W.J. Altwood [47]. SVGA cells provide a BK polyomavirus-free alternative to the parental SVG p12 cell line [46]. Cells were cultured in Dulbecco's modified Eagle's medium (DMEM) (#41965, Thermo Fisher Scientific, Germany) supplemented with 10% fetal bovine serum (FBS) (#P30-3306, PAN-Biotech GmbH, Germany), 1% penicillin–streptomycin (10,000 U/mL, #15140122, Thermo Fisher Scientific), and 2 mM additional L-glutamine (#56-85-9, Carl Roth, Germany) and then incubated at 5% CO_2 at 37°C. Cells were routinely checked for mycoplasma contamination by qPCR (#11-1100, Venor GeM Classic; Minerva Biolabs, Germany).

2.2 | Thin-Film Fabrication

Structured free-standing NiTi films were fabricated by patterning using photolithography (Karl Suss MA6, Germany), wet chemical etching of the sacrificial layer of copper, and magnetron sputtering, described in detail by Bechtold et al. [48] All depositions were carried out in a cluster magnetron sputter device,

Von Ardenne CS730S (Von Ardenne, Germany). NiTi films were deposited with a thickness of 40 μm from a 4-in. $TiNi_{46.5}$ target (Ingpuls GmbH, Germany) at 2×10^{-3} mbar pressure, 20 sccm argon (Ar) flow, and 150 W at a deposition rate of 3 μm/h.

Rapid thermal annealing (RTA) (CreaTec RTA-6 SY09, Germany) was used to heat treat free-standing NiTi structures. The chamber was under a vacuum at 1.0×10^{-7} mbar and the heat treatments were performed at 700°C for 600 s. This step is essential for material to crystallization amorphous, sputtered NiTi. The treated samples were checked to determine whether they were fully crystallized and showed superelastic behavior, as for commercial neuronal implants as shown in Figure S1.

After heat treatment, a 500 nm SiO_2 layer was deposited onto crystalline NiTi as an insulation layer by radio frequency (RF) sputtering, parameters 3×10^{-3} mbar pressure, 30 sccm Ar flow, and 50 W power at a deposition rate of 0.3 μm/h with a 4-in. target (Evochem Advance Materials, Germany). Wafers were cooled down for 4 h in the chamber under vacuum. On top of SiO_2, commonly used electrode materials Au and Pt were deposited with 10 nm chromium and tantalum adhesion layers, respectively. Chromium sputtering parameters for the 8-in. target (Evochem Advance Materials) were 4×10^{-3} mbar pressure, 25 sccm Ar flow, and 200 W power at a deposition rate of 3.3 μm/h, Au parameters 6×10^{-3} mbar pressure, 25 sccm Ar flow, and 100 W power with at a deposition rate of 7.2 μm/h for a 4-in. target (Evochem Advance Materials). Tantalum sputtering parameters for an 8-in. target (Kurt J. Lesker Company, Germany) were 4×10^{-3} mbar pressure, 30 sccm Ar flow, and 200 W power at a deposition rate of 2.2 μm/h, Pt parameters 8×10^{-3} mbar pressure, 25 sccm Ar flow, and 100 W at a deposition rate of 3.7 μm/h for a 4-in. target (Evochem Advance Materials). The temperatures on these samples were measured from below the wafer using temperature C-type stripes from Carl Roth (Carl Roth GmbH). Au and Pt wafer temperatures were recorded as 182°C ± 5°C and 187°C ± 5°C, respectively.

2.3 | Drug Treatment

TβRI kinase inhibitor, SB431542, was obtained from Sigma-Aldrich/Merck (#616461, Sigma-Aldrich/Merck, Germany) and used at a concentration of 1 μM. The TβRII-selective degrader 1b (i.e., active (*R*)- and inactive (*S*)-enantiomer) was prepared as we have described previously [49] and used at a concentration of 2.5 μM. The different compounds were dissolved in polyethylene glycol 400 (PEG400) (Caesar & Loretz GmbH, Germany). The compounds showed no toxic effect on astrocytes (SVGA) (Figure S2). SVGA astrocytes were seeded in 12-well plates at a density of 7500 cells per well. After 24 h, astrocytes were pre-incubated with the different drug compounds 30 min before the NiTi/TGFβ treatment.

2.4 | Quantitative Polymerase Chain Reaction (qPCR)

SVGA astrocytes were seeded in 12-well plates (7500 cells/well) and left to adhere for 24 h. Afterwards, 10 ng/mL recombinant human TGFβ1 (#11343160, ImmunoTools, Germany) and NiTi were added. NiTi was submerged into the media, allowing it to rest atop the cultured cells at the bottom of the well. Medium was renewed on Days 3 and 6. After 7 days, cells were harvested and homogenized using the TRI Reagent (#T9424, Sigma-Aldrich/Merck) and total ribonucleic acid (RNA) was isolated, following the manufacturer's protocol. Then, genomic deoxyribonucleic acid (DNA) was digested using RNase-free DNase (1 U/μL, #89836, Thermo Fisher Scientific) and cDNA was synthesized with the RevertAid RT Kit (#K1691, Thermo Fisher Scientific). TaqMan primers and probes (Thermo Fisher Scientific) and HOT FIREPol Probe Universal qPCR Mix (#08-17-00001, Solis BioDyne, Estonia) were used to analyze samples with the ABI PRISM 7500 sequence detection system (Applied Biosystems). The following genes were analyzed: GAPDH (Hs99999905_m1), IL6 (Hs00985639_m1), FN1 (Hs00277509_m1), and BGN (Hs00959143_m1).

For the TaqMan Array Human TGFB Pathway (#4414097, Thermo Fisher Scientific) samples were prepared as described above, processed according to the manufacturer's protocol, and analyzed with the ABI PRISM 7300 sequence detection system (Applied Biosystems).

The cycle threshold (Ct) values were determined through the instrument software, and ΔCt values = Ct[gene of interest] − Ct[GAPDH] were calculated. Due to the logarithmic reaction mode, a ΔCt value of 3.33 corresponds to gene expression that is one order of magnitude lower than GAPDH. For cytokine-induced mRNA regulation, ΔΔCt values were calculated as follows: $\Delta\Delta Ct = 2^{-(\Delta Ct[\text{stimulus}]-\Delta Ct[\text{control}])}$.

2.5 | Fluorescent Staining/Immunocytochemistry

NiTi was glued to glass coverslips using Kwik-Sil silicone elastomer (World Precision Instruments, Germany) and dried for 24 h at room temperature. SVGA astrocytes were seeded on the glass coverslips (30,000 cells/coverslip) and placed in 6-well plates; then recombinant human TGFβ1 (10 ng/mL) was added and the cells were subsequently incubated for 7 days. Medium was renewed on days 1 and 4. On day 7, cells were briefly rinsed with phosphate-buffered saline (PBS) and fixed for 10 min in 4% paraformaldehyde (PFA, in PBS) at room temperature. Immunocytochemistry was carried out after permeabilization with 0.1% Triton X-100 (Sigma-Aldrich/Merck) in PBS for 5 min at room temperature and blocking for 60 min in bovine serum albumin (BSA, 0.5%, Biomol, Germany) and glycine (0.5%, Carl Roth) in PBS. The cultures were then incubated with primary antibodies in PBS at 4°C overnight, anti-galectin-3 (goat, 1:100; #AF1154, Bio-Techne GmbH, Germany) was used as the primary antibody. Then, cells were incubated with Alexa Fluor 555-labeled secondary antibodies against respective host species (donkey IgG, 1:1000, Thermo Fisher Scientific) at 37°C for 1 h, and nuclei were counterstained with 4′,6-diamidino-2-phenylindole (DAPI) (Sigma-Aldrich/Merck). Slides were embedded with Shandon Immu-Mount (#FIS9990402, Thermo Fisher Scientific). For secondary antibody controls, primary antibodies were omitted (Figure S3). Imaging was carried out using the Keyence BZx800 Fluorescence Microscope (KEYENCE GmbH, Germany). Fluorescence intensity was quantified using ImageJ (RRID: SCR_003070) [50].

For ECM fluorescence staining, cells were briefly rinsed with PBS and fixed for 10 min in 4% PFA (in PBS) at room temperature. The labeling was performed with biotinylated *Wisteria floribunda* lectin (WFL) (1:100, #B-1355, RRID: AB_2336874, Vector Laboratories, USA) at room temperature for 1 h followed by incubation with Cy3-conjugated Egg-white Avidin (1:200, #003-160-083, Jackson Immuno Research, UK) at 37°C for 1 h, and nuclei were counterstained with DAPI (#D9542, Sigma-Aldrich/Merck). Afterwards, samples were imaged using fluorescence microscope as described previously.

2.6 | Scanning Electron Microscopy (SEM)

NiTi was glued to glass coverslips using Kwik-Sil silicone elastomer (World Precision Instruments) and dried for 24 h at room temperature. SVGA astrocytes were seeded (30,000 cells/well) on the coverslips placed in 6-well plates. Next, recombinant human TGFβ1 (10 ng/mL) was added and the cells incubated for 7 days. Medium was renewed on days 1 and 4. After 7 days, cells were washed with PBS and fixed for 30 min in 3% glutaraldehyde (in PBS). Samples were then rinsed with PBS and submerged in a 2% osmium solution for 20 min. Subsequently, all water content was removed via serial dehydration using ethanol (30%–100%), followed by critical point drying using a CPD 030 (Bal-Tec, Balzers, Liechtenstein). Finally, samples were sputter coated with Au (SCD 050 sputter coater, Bal-tec, Balzers, Liechtenstein) for 50 s, and imaged using a JSM-IT200 (JEOL, Germany). Pristine NiTi and Au, Pt coated NiTi thin films were imaged on specimens by using Zeiss Ultra 55 Plus (Zeiss, Germany) with 3 keV. Samples were fixed onto SEM holders by using carbon tape.

2.7 | Atomic Force Microscopy (AFM)

AFM measurements were obtained on an SPM 1000 instrument (AIST-NP, USA) in tapping mode. Samples were fixed on the stage using carbon tape. Measurements were conducted at room temperature.

2.8 | Contact Angle and Surface Energy

Contact angle measurements of deionized water (DI) and dimethyl sulfoxide (DMSO, Thermo Scientific) were measured twice using the sessile drop method with a volume of 5 μL. The goniometer testing apparatus was an in-house setup while the measurements were analyzed with National Instruments LabView (National Instruments Corp, USA). Measurements were performed at room temperature. For surface energy calculations, Young's equation (1) and QWRK equation (2) were used [51]. Table 1 and Equations (1) and (2) show the surface tension values of the solvents that were used to calculate the surface energy of sputtered thin films.

$$\gamma_S = \gamma_{SL} + \gamma_L \cos\theta \tag{1}$$

$$\gamma_{SL} = \gamma_S + \gamma_L - 2\left(\sqrt{\gamma_S^D \gamma_L^D} + \sqrt{\gamma_S^P \gamma_L^P}\right) \tag{2}$$

TABLE 1 | Data used to calculate surface energy [52].

	γ_L	γ_L^D	γ_L^P
DI water (mJ/m^2)	72.8	21.8	51
DMSO (mJ/m^2)	44	36	8

Abbreviations: DI, Deionized water; DMSO, Dimethyl sulfoxide.

2.9 | Statistical Analysis

All results are presented as mean values ± standard deviation (SD) and numbers of biological replicates are stated in the respective figure legends. Statistical analysis was performed using GraphPad Prism V9.4.1 (RRID: SCR_002798). Statistically significant differences were evaluated by one-way analysis of variance (ANOVA), followed by Tukey's post hoc test for comparisons between multiple groups. Statistical significance was set at p-value of 0.05.

3 | Results

3.1 | Establishing and Characterizing an In Vitro Glial Scar Model

To develop an in vitro glial scar model, human SVGA astrocytes were subjected to alternative activation using TGFβ, and incubation with magnetron-sputtered NiTi free-standing thin films for 7 days. This time frame was chosen because after 7 days substantial astrocytic reactivity was previously found in in vivo studies and the acute foreign body response shifts to visible glial scarring [53]. Glial scars are characterized by a substantial accumulation of extracellular matrix (ECM) proteins, most notably astrocyte-derived glycosaminoglycan (GAG)-rich chondroitin sulfate proteoglycans (CSPGs) [6]. Consequently, human SVGA astrocytes were stained for overall ECM proteins following incubation with NiTi thin films, activation with TGFβ, or a combination of the two. WFL staining did not reveal any notable changes in ECM protein production between untreated controls and astrocytes incubated with NiTi thin films or TGFβ-activated astrocytes alone. In contrast, astrocytes treated with both NiTi thin films and TGFβ displayed an almost three fold increase in fluorescence intensity per cell after WFL staining ($p < 0.0001$) (Figure 1a,b). This suggests that only the combination of TGFβ-activated astrocytes incubated with NiTi thin films induces glial scar-like behavior in astrocytes. Additionally, as illustrated in Figure 1c, astrocytes begin to grow on the NiTi thin film in combination with TGFβ treatment, forming a glial scar-like tight sheet around it. Moreover, TGFβ-treated astrocytes in contact with NiTi surfaces appear flatter, with noticeably larger cell bodies. In contrast, untreated control cells exhibit a more filamentous morphology, with smaller cell bodies covering less surface area (Figure 1c).

Glial scars create an inflammatory microenvironment in their vicinity [8, 54]. To assess pro-inflammatory processes, astrocytes were stained for galectin-3 after TGFβ/NiTi thin-film treatment. Galectin-3 is emerging as a biomarker for neuroinflammation and astrocyte reactivity [55, 56]. The fluorescence intensity per cell in astrocytes treated with TGFβ/NiTi thin films increased

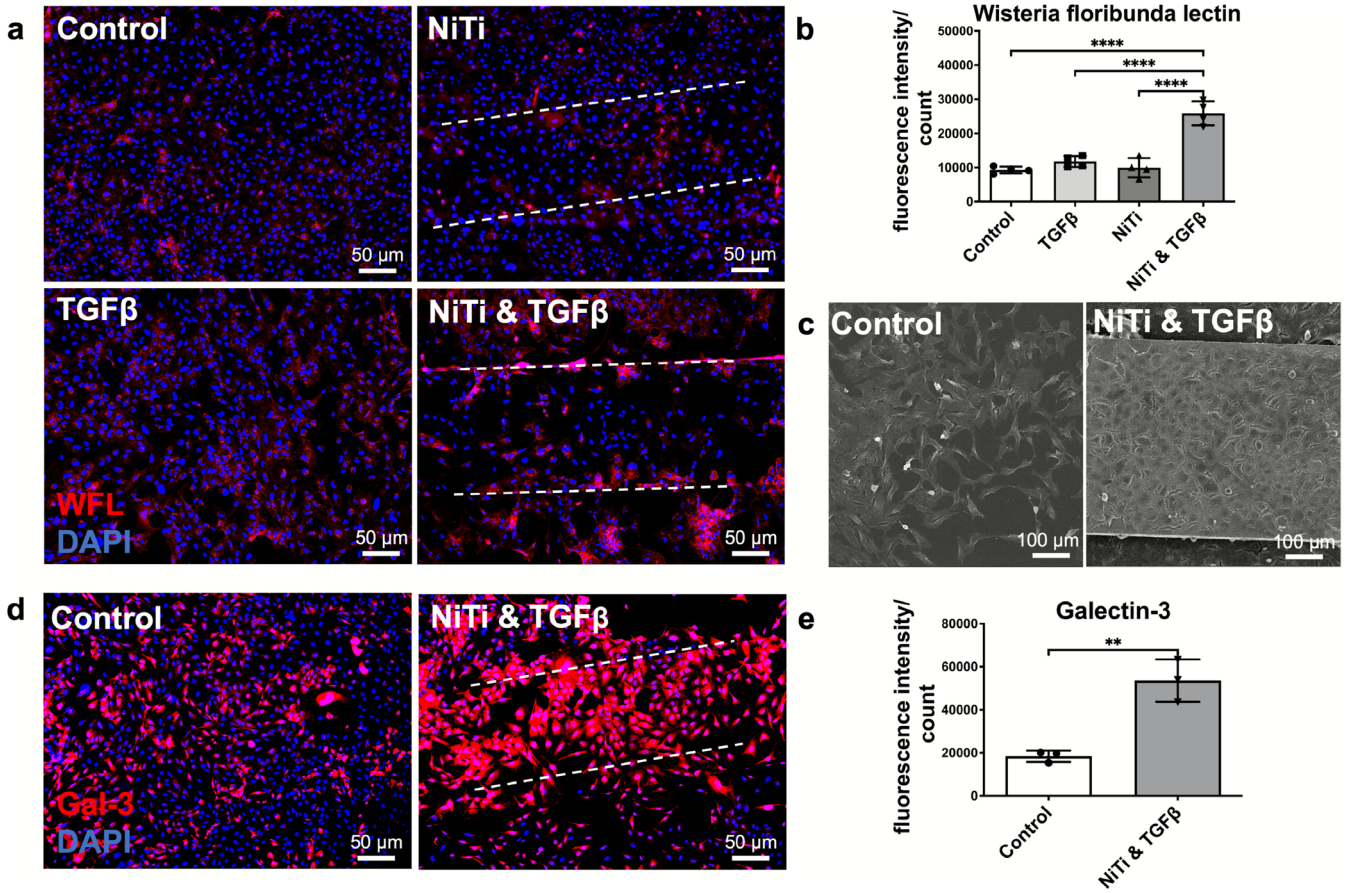

FIGURE 1 | In vitro glial scar formation. (a) Representative fluorescence staining images of *Wisteria floribunda* lectin (WFL, red) and nucleus (DAPI, blue) in SVGA showed an accumulation of ECM proteins in NiTi thin films and transforming growth factor β (TGFβ)-treated samples compared to unstimulated controls, NiTi thin films, or TGFβ alone. Dotted lines represent the borders of the NiTi films. (b) Corresponding quantification of fluorescence intensity of cells both inside and outside the dotted lines normalized to cell number. (c) Representative scanning electron microscopic images displaying the cell growth on the NiTi thin film compared to untreated controls. (d) Representative fluorescence staining images of galectin-3 (Gal-3) (red) and nucleus (DAPI, blue) in SVGA showed an increase in galectin-3 expression in NiTi thin films and TGFβ-stimulated samples compared to unstimulated controls. Dotted lines represent the borders of the NiTi films. (e) Corresponding quantification of fluorescence intensity normalized to cell number. (a, b, c, d, e) $n => 3$ no. of independent cell cultures; significance set at $^{**}p < 0.01$, and $^{****}p < 0.0001$.

by more than double ($p < 0.01$) compared to untreated controls (Figure 1d,e). The elevated accumulation of ECM proteins, changes in cell growth patterns, and the neuroinflammatory environment collectively indicate that TGFβ/NiTi thin-film treatment triggers the formation of glial scars in astrocytes.

3.2 | Pharmacological Inhibition of TGFβ Signaling Reduces ECM-Protein Expression in Human SVGA Astrocytes

In the next steps, the established in vitro glial scar model was employed to assess various strategies aimed at mitigating glial scarring. In the first approach, two mechanistically distinct small-molecule TGFβ inhibitors were utilized. SB431542 targets the kinase domain of the type I TGFβ receptors (TβRI) (i.e., activating receptor-like kinases ALK-4, -5, and -7) [57]. For perturbation of type II TGFβ receptors (TβRII), we used the class of *b*-annealed dihydropyridines that do not affect the kinase domains, but rather induce the proteasomal degradation of type II receptor without affecting the type I receptor. Antifibrotic activities have been demonstrated for these compounds in various models in vitro and in vivo [58–60]. Structure–activity relationship (SAR) studies furnished high-quality pharmacological tool compounds for these TβRII degraders with active *R*-enantiomers and inactive *S*-enantiomers as optimal controls [49, 61]. Here, we employed the SAR-optimized 1b as single enantiomers and first profiled their anti-fibrotic efficacy in the glial scar model by qPCR [49]. Transcriptional changes can often be proceed detectable changes at the protein level and therefore provide valuable insights into cellular responses. Astrocytes were pre incubated for 30 min with SB431542 (1 µM) and the 1b enantiomers (2.5 µM). The concentrations of SB431542 [62] and the 1b enantiomers [49] were chosen based on previous literature to ensure that pathways were effectively modulated while maintaining cellular health and avoiding off-target effects. After another 7 days of TGFβ/NiTi thin-film treatment, gene expression of the specific glial scar-associated ECM proteins biglycan, representative for the group of CSPG, and fibronectin was analyzed [63, 64]. In comparison to untreated controls, messenger ribonucleic acid (mRNA) levels of both biglycan and fibronectin were significantly elevated after TGFβ/NiTi thin-film treatment ($\Delta\Delta$Ct Bgn = 3.5 ± 1, $\Delta\Delta$Ct Fib = 5.5 ± 0.5) (Figure 2). Astrocytes

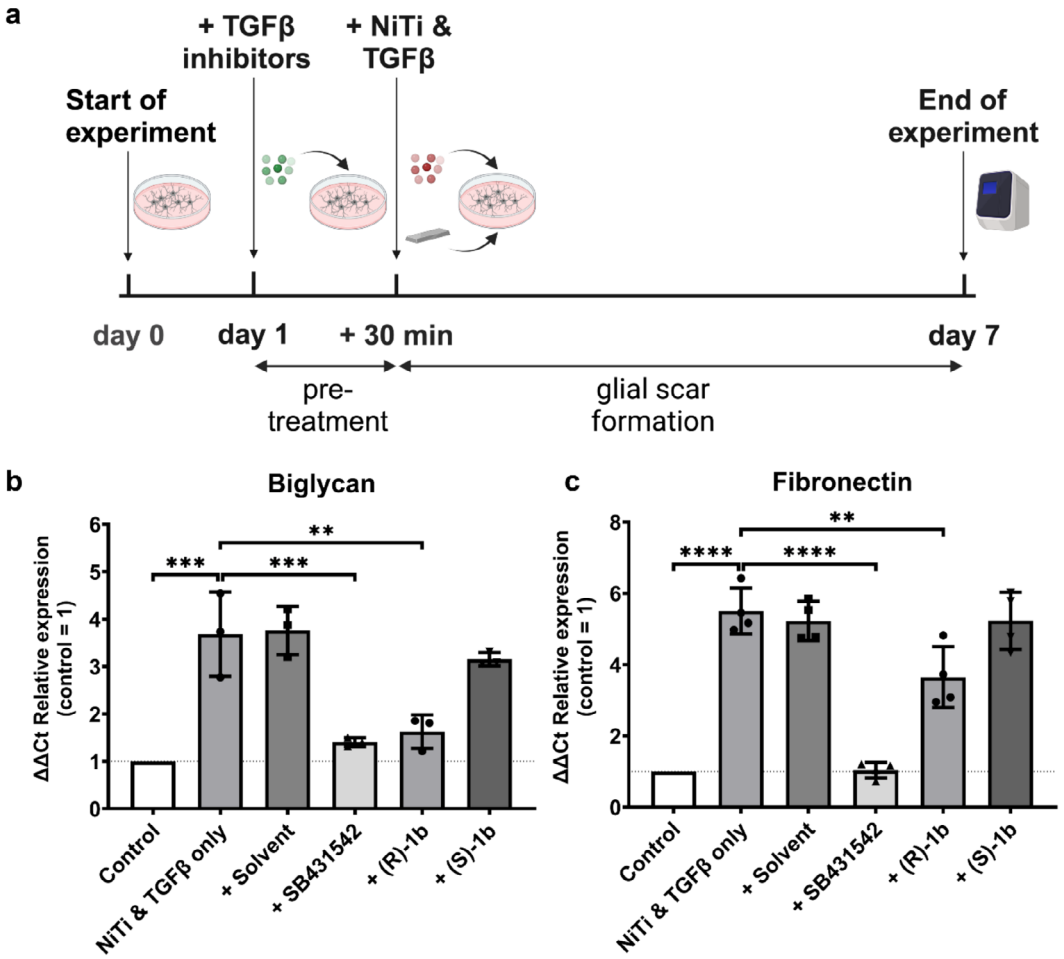

FIGURE 2 | Influence of transforming growth factor β (TGFβ) receptor perturbation on glial scar-associated gene expression. (a) Illustration of the experimental sequence. (b, c) Quantitative polymerase chain reaction analysis indicates increased gene expression levels of biglycan and fibronectin after NiTi thin films and TGFβ stimulation compared to untreated controls. TβRI inhibitor (SB431542) and TβRII inhibitor (R)-1b each independently reduced gene induction of biglycan and fibronectin. (S)-1b is the inactive enantiomer as a negative control. (b, c) $n => 3$ no. of independent cell cultures; significance set at $^{**}p < 0.01$, $^{***}p < 0.001$, $^{****}p < 0.0001$.

additionally incubated with SB431542 exhibited a substantial reduction in gene expression for both biglycan ($p < 0.01$) and fibronectin ($p < 0.0001$) compared to astrocytes treated only with TGFβ/NiTi thin films. Similarly, astrocytes treated with (*R*)-1b, the active enantiomer, demonstrated a significant reduction in biglycan gene expression ($p < 0.01$). Although the reduction in fibronectin gene expression was less pronounced than with SB431542, it remained significant compared to astrocytes treated only with TGFβ/NiTi thin films ($p < 0.05$). In contrast, (*S*)-1b, the inactive derivative, showed no significant effect on biglycan and fibronectin mRNA levels. Hence, modulating the TGFβ receptors was proven to be effective in diminishing ECM protein production in glial scarring, thereby limiting its barrier properties.

3.3 | Elevated Proinflammatory Interleukin 6 as a Key Indicator in the In Vitro Glial Scar Model

To further investigate the involvement of TGFβ pathways in glial scar formation, a multiarray qPCR assay was performed. The results revealed that multiple genes related to the TGFβ pathway were upregulated following treatment with TGFβ/NiTi thin film (Figure S4). Particularly noteworthy was the identification of interleukin 6 (IL6) as the most prominently expressed gene, with the relative mRNA level being 10 fold higher than that of the untreated control (Figure 3a,b). To validate the increased gene expression, a standard qPCR setup was employed. The results plotted in Figure 3b confirm the finding of tenfold increased mRNA levels of IL6 induced by TGFβ/NiTi thin-film incubation compared to untreated controls.

Subsequently, the impact of the two TGFβ receptor inhibitors on IL6 expression were examined. The addition of SB431542 (1 μM) resulted in a significant decrease in IL6 mRNA levels, approaching those of untreated controls and markedly lower than TGFβ/NiTi thin-film treatment alone ($p < 0.001$). Similarly, the addition of (*R*)-1b (2.5 μM) significantly reduced IL6 gene expression ($p < 0.05$), although it remained fivefold higher than in untreated controls. The inactive (*S*)-1b exhibited no significant effect on IL6 mRNA levels compared to TGFβ/NiTi thin-film treatment alone.

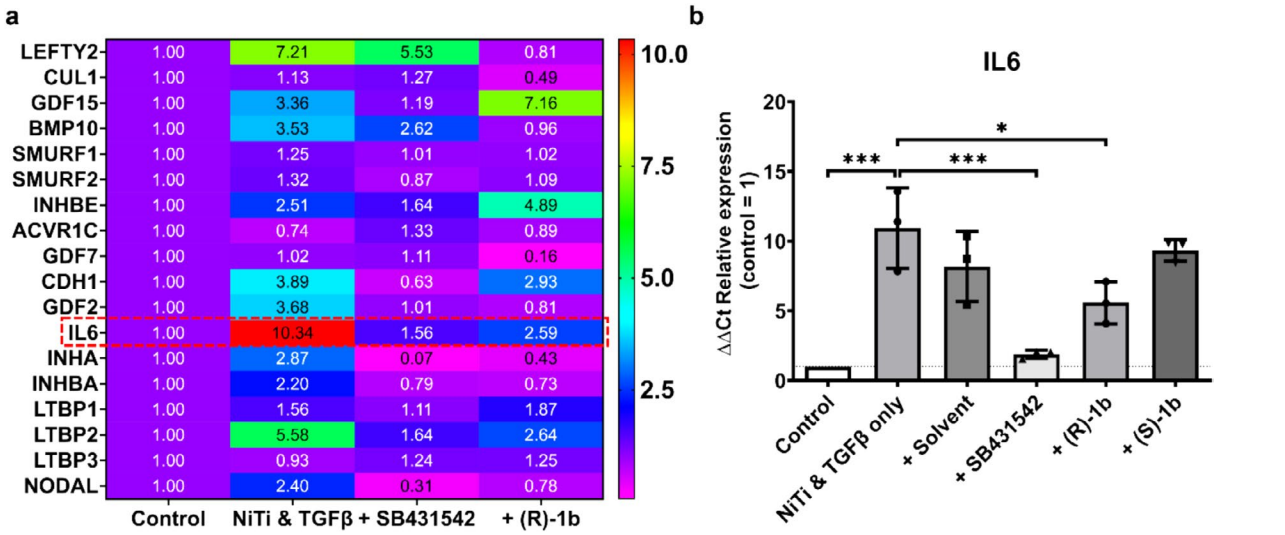

FIGURE 3 | The involvement of IL6 in glial scar formation. (a) Quantitative polymerase chain reaction array of transforming growth factor β (TGFβ) pathway-related genes shows significant upregulation of interleukin 6 (IL6) gene expression (ΔΔCt) after NiTi thin film and TGFβ treatment. (b) Standard qPCR analysis confirms increased levels of IL6 gene expression compared to untreated controls. TGFβ receptor inhibitors reduce the IL6 gene upregulation. (S)-1b is the inactive enantiomer as a negative control. (a, b) $n = > 1$ no. of independent cell cultures, significance set at $^{*}p < 0.05$, and $^{***}p < 0.001$.

These findings underscore the substantial upregulation of proinflammatory biomarker IL6 in the in vitro glial scar model that we established. Furthermore, it highlights the beneficial effects of both type I and II TGFβ receptor inhibitors not only on ECM protein accumulation but also on the production of proinflammatory cytokines.

3.4 | Material Modifications Impact Surface Roughness and Surface Energy

Apart from the assessment and validation of new drug targets to reduce glial scar formation, the model can also be applied to investigate further variables affecting glial scarring. One significant factor in developing neural implant is the material properties of the implant and especially its surface, since as the implant will be in direct contact to the surrounding tissue [17, 65]. Surface characteristics such as topography, surface roughness, surface groove size and orientation, surface porosity, and distribution can have a strong influence on the adhesion, migration, proliferation, and differentiation of cells after injury [66].

In this study, NiTi thin films were used as a substrate and their surface properties were modulated using different coatings. Au and Pt, common materials used as neuronal electrodes [18, 67, 68], were deposited on the NiTi backbone substrate by sputter coating to create electrodes, with SiO_2 deposited as an insulator in between the NiTi and electrode materials [24]. Afterwards, surface roughness and energy of free-standing NiTi, NiTi-SiO_2, NiTi-SiO_2-Au, and NiTi-SiO_2-Pt were investigated by using scanning electron microscopy (SEM), atomic force microscopy (AFM), and static contact angle; consequently, the surface energy was calculated. The cell studies were omitted for NiTi-SiO_2 samples since SiO_2 was only added as an insulation layer. The material properties of NiTi-SiO_2 are presented in Figure S5.

Figure 4a illustrates the deposited layers on free-standing NiTi. SEM analyses revealed that the surface morphology was different for the various coatings. SEM images were taken of free-standing NiTi (Figure 4b) and Au (Figure 4c) and Pt (Figure 4d) electrode materials deposited on NiTi-SiO_2. These images depict a clear texture change on the surface. The microstructure of the thin films is examined as four zones based on the substrate temperature (Ts) and the melting point (Tm) of the sputtered material: Zone I ($Ts/Tm < 0.1$), Zone T ($0.1 < Ts/Tm < 0.3$), Zone II ($Ts/Tm > 0.3$), and Zone III structure at higher temperatures [69]. During sputtering of Au and Pt electrodes, the temperatures of the substrates were measured as 182°C ± 5°C and 187°C ± 5°C and the melting points of Au and Pt were 1064°C and 1769°C, respectively [69, 70]. This results in Ts/Tm of 0.17 and 0.11, respectively. Both are in Zone T when considering the Ar pressure used during sputtering, which may be linked to the similarities in surface roughness range. Salvadori et al. showed that Pt has smaller grain sizes than Au under the same deposition parameters on silicon substrates [71].

Nevertheless, SEM alone cannot fully capture the surface topography; therefore, AFM was used for further analysis to determine surface roughness. The root-mean-square (RMS) values and AFM images are shown in Figure 4e. The free-standing NiTi exhibits a more uniform surface; yet, AFM analysis reveals it has the roughest surface with an RMS value of 7.5 nm. However, the roughness values of the other samples are close in comparison to NiTi. Only clear petal-like (circular) structures of Au and Pt are seen in both SEM and AFM. Pt shows the smoothest surface with RMS values of 5.8 nm compared to the Au surface with 6.5 nm.

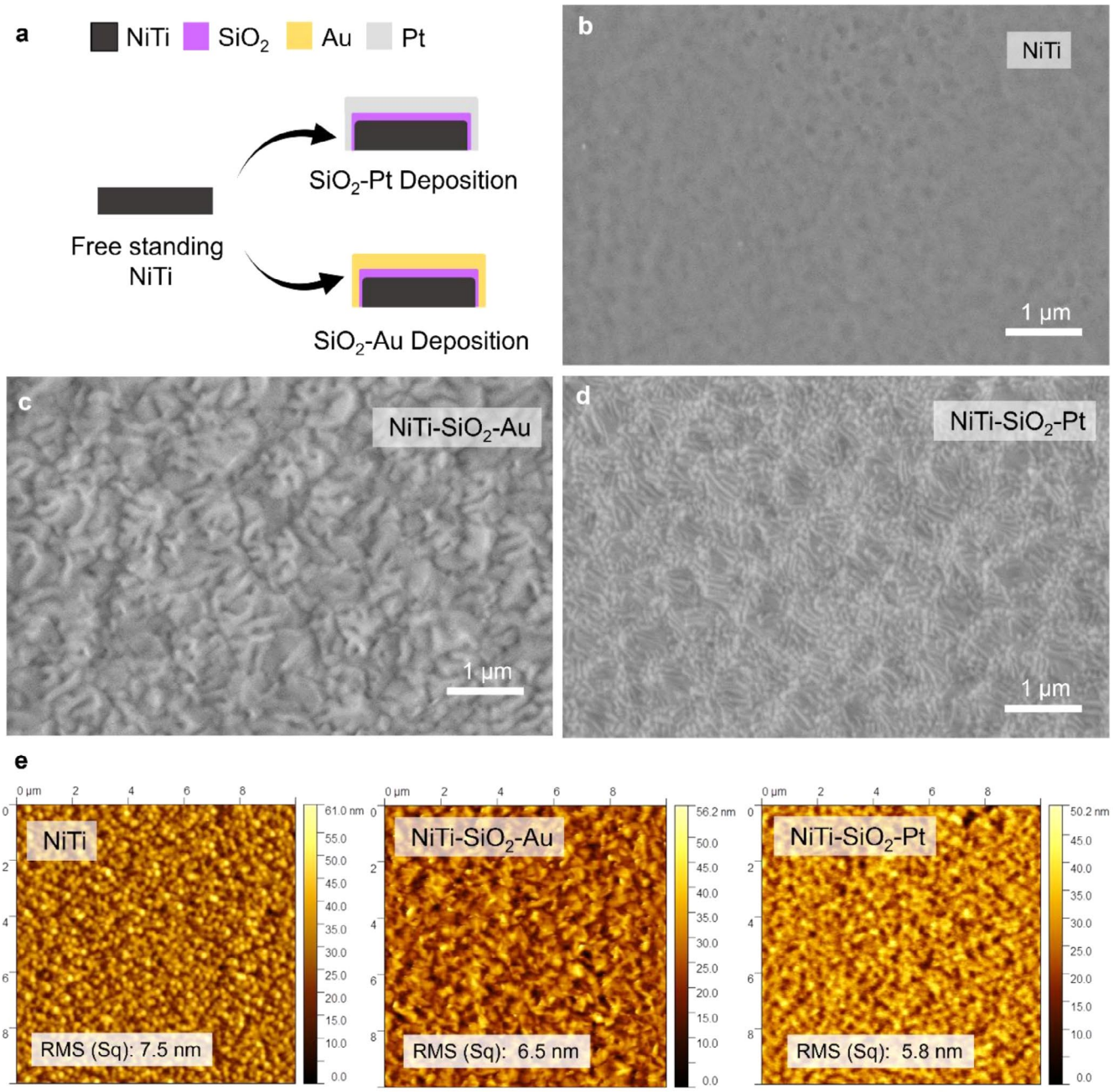

FIGURE 4 | Surface roughness. (a) Illustration of the surface modifications. Representative scanning electron microscopic images of (b) NiTi, (c) NiTi-SiO_2-Au, and (d) NiTi-SiO_2-Pt. (e) Atomic force microscopic results for crystalline NiTi, Au layer sputtered on NiTi-SiO_2 and Pt layer sputtered on NiTi-SiO_2. (b, c, d, e) $n => 1$ no. of independent experiments. RMS, Root-mean-square.

Static contact angle measurements were performed to determine the hydrophobicity of the surface and calculate the surface energy. A material surface is hydrophobic if water contact angles are higher than 90°; if angles are lower than 90°, the surface is hydrophilic [72]. Figure 5 shows that free-standing NiTi has a water contact angle of 95° ± 2°, denoting it as hydrophobic, compared to the more hydrophilic surfaces after coating electrodes with NiTi-SiO_2-Pt (84° ± 4°) and NiTi-SiO_2-Au (65° ± 3°). The surface energies of the stacks are determined by using Equations (1) and (2) with SCA of both DI water and DMSO measured. The surface energies of NiTi, NiTi-SiO_2-Pt, NiTi-SiO_2-Au are 33, 38, and 42 mJ/m^2, respectively.

3.5 | NiTi Thin-Film Modifications Influence ECM Protein Expression in Human SVGA Astrocytes in Combination With TGFβ Signaling Activation

In the final analysis, we explored the impact of Pt and Au sputter coating on free-standing NiTi thin films on glial scar formation. In the established in vitro glial scar model, astrocytes were activated with TGFβ and then incubated for 7 days in combination with either NiTi thin films, Au-coated NiTi thin films, or Pt-coated NiTi thin films. Subsequently, the mRNA levels of ECM proteins biglycan and fibronectin were evaluated by using qPCR (Figure 6). Compared to untreated

controls, NiTi-SiO_2-Au exhibited a significant increase in both biglycan ($p < 0.01$) and fibronectin ($p < 0.01$) gene expression. Free-standing NiTi resulted in lower, but still significantly increased mRNA levels of biglycan ($p < 0.05$) and fibronectin ($p < 0.05$). In contrast, NiTi-SiO_2-Pt led to a significant, but smaller upregulation of fibronectin gene expression ($p < 0.05$), while showing no significant elevation in biglycan mRNA levels. This indicates that Pt-coated NiTi thin films tend to induce less reactivity in astrocytes by reduced ECM protein production and modulating glial scar formation compared to other NiTi thin-film modifications.

4 | Discussion

In-depth investigations of glial scar formation and subsequent therapeutic approaches are subject to ongoing research. The present study describes a human cell line-based in vitro glial scar model and demonstrates its feasibility for investigating the effects of drug treatment or biomaterial modifications by combining innovative chemical fabrication techniques with a complex in vitro co-stimulation system to investigate biological responses at the cell-material interface. In recent years, various research groups, as discussed in the following paragraph, have

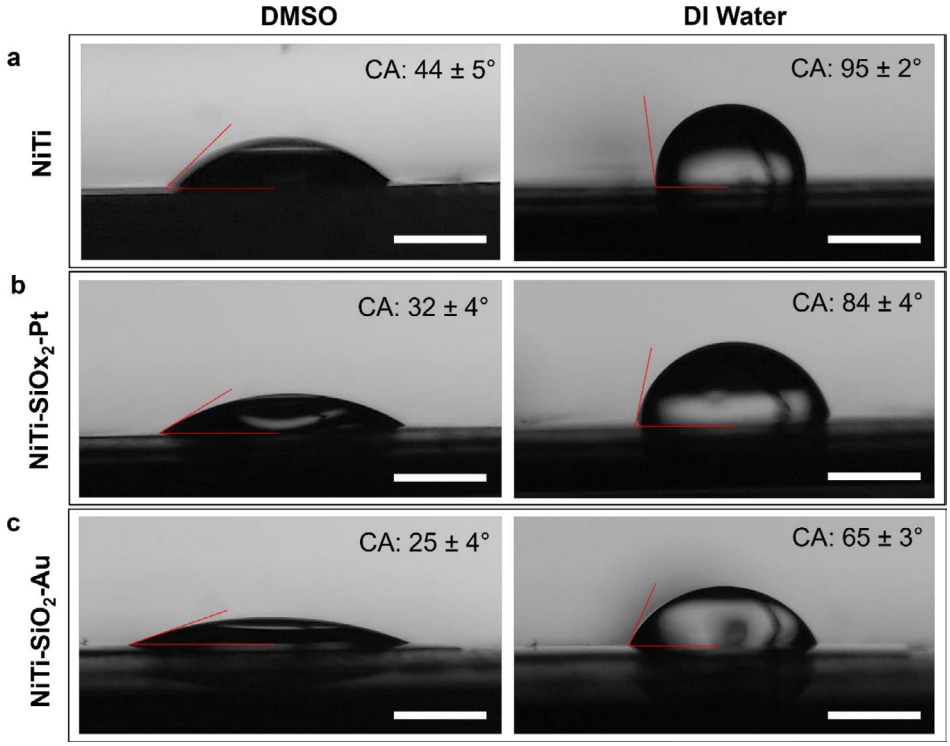

FIGURE 5 | Surface energy. Representative images of static contact angle (SCA) measurements of dimethyl sulfoxide (DMSO) (left) and deionized (DI) water (right) on (a) crystalline NiTi, (b) Pt layer sputtered on NiTi-SiO_2 and (c) Au layer sputtered on NiTi-SiO_2. (a, b, c) $n = 2$ no. of independent experiments.

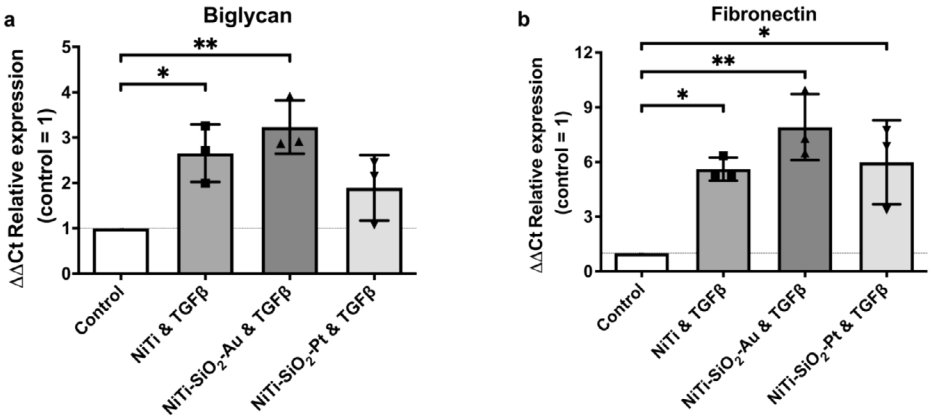

FIGURE 6 | Influence of material surface modification on glial scar-associated gene expression. (a, b) Quantitative polymerase chain reaction analysis indicates differences in gene expression level induction of biglycan and fibronectin for NiTi thin films coated with Au, Pt, or uncoated combined with transforming growth factor β (TGFβ) stimulation compared to untreated controls. (a, b) $n = 3$ no. of independent cell cultures; significance set at $^*p < 0.05$, $^{**}p < 0.01$.

successfully developed in vitro models that mimic the features of glial scars. These comprehensive in vitro models offer a distinct advantage by providing a high degree of experimental control [73], which not only minimizes the need for ethically questionable in vivo glial scar models in rodents [74, 75] but also positions them as invaluable, initial testing platforms for assessing the efficacy of new materials or drugs [26].

Oxygen glucose deprivation (OGD) [76, 77] or mechanical stretching [78] of astrocytes has been demonstrated to induce changes reminiscent of glial scar formation. While these approaches serve well in modeling glial scarring after events such as stroke or traumatic brain injury, they lack a representation of an implanted foreign body, which might be a crucial aspect. Polikov et al. addressed this issue by introducing a model of glial scarring that involves inserting a stainless steel microwire as a foreign body into a mixed primary glial culture. Within a short span of 10 days, they observed the formation of a glial scar around the stainless steel microwire [33]. This in vitro model was subsequently refined to explore the biocompatibility of various coatings deposited on the stainless steel microwire [79]. In another innovative approach, glial scarring was induced in a 3D culture system by inserting a glass probe into primary mixed glial cells cultivated in a collagen gel [31]. However, stainless steel or glass materials are rarely employed for actual neural implants. In contrast, NiTi is emerging as a promising material for brain-machine interface applications and, as such, the neural response to this material is currently under extensive investigation [24, 80]. Therefore, the in vitro glial scar model presented in this study builds upon previously established platforms but advances them to the next level by incorporating NiTi and human cells, thereby enhancing the relevance and applicability of the model.

The formation of glial scars not only arises as a cellular response to materials but also stems from a complex interplay among various brain cells. Activated microglial cells are known to initiate reactivity in astrocytes by releasing specific factors [81]. These factors, capable of inducing reactive astrocytes in vitro [12] are integral in the complex process of scar formation. TGFβ stands out as a key modulator in this context, as it alternately activates astrocytes, promoting their (in a simplified description) transition into the A2 state [13, 82]. While TGFβ-mediated glial scarring is not the only relevant pathway for glial scar formation, previous studies have highlighted its importance. Indeed, Song et al. demonstrated that macrophages induce glial scar formation through TGFβ secretion [83]. Similarly, Bellver-Landete et al. found a correlation between TGFβ expression and microglial scar formation following spinal cord injury [2]. In line with these findings, we used the "alternative" TGFβ pathway to create a controlled and reproducible baseline for astrocyte reactivity, resulting in an observable shift into their scar-forming state. Notably, astrocytes exhibited a heightened production of glial scar-associated ECM proteins, but only in conjunction with NiTi placement. This emphasizes the significance of incorporating cellular activation in glial scar testing for materials intended for neural implants. Nevertheless, in future studies further cellular crosstalk and involved pathways should be included.

Beyond the induced deposition of glial scar-forming ECM proteins after TGFβ and NiTi treatment, galectin-3 production was also increased. Galectin-3, recognized as an emerging biomarker in neural diseases, has been shown to play roles in inflammation and microglial activation [84]. Moreover, elevated levels of galectin-3 have also been associated with corneal scarring [85] and renal fibrosis [86]. These findings highlight that the established in vitro glial scar model successfully replicates key features of glial scar formation, including inflammatory factors and increased accumulation of ECM proteins.

The platform introduced in this study was further employed to explore different strategies aimed at mitigating glial scar formation. Inhibition of TGFβ has proven effective in diminishing fibrosis and scar formation in the CNS [63, 87]. Additionally, Hellal et al. demonstrated that paclitaxel reduces scarring after spinal cord injury and expedites axonal regeneration by inhibiting the TGFβ receptor pathway [45]. Building on these findings, pharmacological perturbation of the TGFβ receptor was found to significantly reduce expression of genes associated with glial scar formation. Notably, pathway activation relies on TGFβ binding to TβRII, which phosphorylates TβRI [88]. Although the TβRII/I complex initiates signal transduction through canonical (= SMAD) and noncanonical (e.g., MAPK, PI3K/Akt, or Par6/βPKC) pathways, each receptor has specific functions [89–91]. While effective TβRII inhibitors are expected to inhibit all TGFβ downstream events, TβRI kinase inhibitors largely block canonical signaling fates. In the context of glial scar formation, we surprisingly found that TβRI kinase inhibitor SB431542 exhibited a more pronounced effect than the targeted degradation of TβRII by (*R*)-1b. This is a key finding and it is worth noting that SB431542 is known to interact with a broader range of cellular mechanisms, not solely inhibiting the TβRI receptor [92, 93], which might lead to novel pharmacological approaches to managing glial scar formation in the future.

Furthermore, a broader exploration of different TGFβ pathway-associated genes revealed a substantial upregulation of proinflammatory IL6 following TGFβ/NiTi treatment. This contradicts previous studies reporting that TGFβ inhibits cytokine production in astrocytes [94] and supports a neuroprotective astrocytic state [95]. The discrepancy could be attributed to the combination in the glial scar model of TGFβ activation with NiTi thin films as a foreign body presented in our study, highlighting the need to include cellular crosstalk factors into solely material-cell reaction studies. Furthermore, these results underscore the limitations of the dichotomized classification of reactive astrocytes into proinflammatory/neurotoxic (A1) versus tissue healing/neuroprotective (A2). Astrocytes, being highly dynamic cells, can initiate glial scar formation while still contributing to neuroinflammatory processes.

In addition to pharmacological strategies to ease foreign body reactions and subsequent glial scar formation, an in-depth validation of neural implant materials is imperative. Previously, Chluba et al. proved that NiTi can be used as a substrate for microelectrodes. They studied biocompatibility and cell adhesion on a microfabricated thin-film insulating oxide layer sandwiched between substrate NiTi and a Pt electrode on human endothelial cells (HUVEC) [24]. However, they did not further investigate surface property effects of these materials on the cells, despite the fact that the surface properties of a neuronal implant material are crucial in influencing glial scar formation. Lifeng et al. analyzed the surface properties of NiTi in more

detail to see the effect on genes associated with cell adhesion and inflammation. They found that a titanium nitride (TiN) coating on NiTi increases surface hydrophilicity and total surface energy. This resulted in upregulation of genes related to cell adhesion and inflammation. Nevertheless, they also used HUVEC for their experiments [37].

To increase our understanding of the effects induced by NiTi surface properties on human astrocytes, surface roughness and surface energy were investigated to determine the relationship with protein expressions of glial scar-associated genes (i.e., biglycan and fibronectin). Nevertheless, the relationship between these two parameters is complex. Previous studies showed that surface roughness and surface hydrophobicity, which can be used to determine surface energy, could influence cellular responses to implants. Moreover, it has been recognized that many additional surface parameters, such as surface chemistry and surface charge, play a role in foreign body responses [96–99].

In the present study, free-standing NiTi was found to have the roughest surface but showed the lowest surface energy, which indicates a rather hydrophobic surface. Pt coating displayed the smoothest surface with an intermediate surface energy, while Au coating led to a moderate surface roughness with the highest surface energy and is therefore mostly hydrophilic. However, the surface roughness values found were still relatively close to each other, indicating that surface roughness might not have a profound effect on cellular responses. This correlates to a previous study by Markoff et el. [100] in which they investigated bulk forged Ti-6Al-4V, selective laser melted (SLM) Ti-6Al-4V, and NiTi alloys with and without diamond-like-carbon (DLC) coating for their inflammatory responses and biocompatibility by using human osteoblasts, fibroblasts, and macrophages. Also, the reported inflammatory reactions are unaffected by surface roughness on these cell types. Moreover Svensson et al. [101] showed that modulating the roughness of nanostructured Au surfaces did not affect inflammatory responses. However, they reported that increased surface nano-roughness, which enhances hydrophilicity, could reduce bacterial adhesion. In line with these studies on Au surfaces, Pennisi et al. [102] showed for Pt surfaces that changing the roughness on the surface did not result in a significant influence on fibronectin gene expressions in fibroblasts. Therefore, as these studies have shown, surface roughness might not be the key influence on the cellular responses to NiTi, Pt, and Au surfaces. In line with the findings from the present study, where surface roughness results were found to be close to each other, surface energy and hydrophobicity might be more strongly involved in generating cellular reposes.

Increasing the surface hydrophilicity and total surface energy upregulates genes related to cell adhesion and inflammation [37]. The Au ssurface, characterized by high surface energy, induced notable upregulation of fibronectin and biglycan gene expression. However, although NiTi had the lowest surface energy, Pt showed lower glial scar-associated gene expression. The reason for this could be related to the surface chemistry influencing inflammatory gene expression [13, 103, 104]. It is known that NiTi has a native titanium dioxide (TiO_2) layer on its surface [105]. Feng et al. [106] previously investigated the effects of surface hydroxyl groups on rabbit osteoblasts by altering the oxide layer of titanium surfaces. They reported that higher levels of oxidation increase roughness, surface energy, and presence of hydroxyl groups. These surface properties all fostered greater adhesion of cells and could influence the cell response to free-standing NiTi. This result could explain why Pt induces less protein expression correlated to glial scarring compared to NiTi. In addition, another study by Ereifej et al. [107] demonstrated the beneficial effects on cellular responses by examining glial scar responses and biocompatibility of Pt alloy wires compared to iridium (IV) oxide (IrO_2). Their results indicated that the platinum alloy wires induced less reactivity in astrocytes. However, they did not investigate surface roughness or energy. Further studies on surface structure and chemistry are required to fully understand the behavior of sputtered thin films on astrocyte reactivity.

While the established glial scar model used in this study provides valuable insights, some limitations must be acknowledged. One key limitation to ensure the platform's simplicity and high reproducibility is the exclusion of other relevant cell types, especially microglia and neurons, which play critical roles in glial scar formation and in the overall neural tissue response, constituting a key limitation. Additionally, the model employs a 2D culture system, which, although useful for controlled analysis of cellular behavior, does not fully capture the 3D complexity of in vivo neural environments. Another constraint is the model's focus on TGFβ-mediated pathways, which, while important, does not encompass the broader spectrum of signaling mechanisms involved in glial scar formation. Nevertheless, by focusing on TGFβ-mediated glial scarring enables for studying a specific pathway rather than endeavor to comprehensively simulate all scarring mechanisms.

Furthermore, although surface parameters such as roughness and surface energy were comprehensively investigated, the absence of a detailed analysis of surface chemistry represents an additional limitation. Lastly, the model does not replicate the dynamic mechanical forces present within the brain, such as those induced by pulsatile blood flow or physical strain, which may influence the cellular response. These limitations highlight the need to further refine the model to enhance its physiological relevance, while underscoring the strengths of our approach in establishing an easy-to-use and reliable platform for initial biomaterial or drug testing in vitro.

5 | Conclusion

In summary, the in vitro glial scar model established in the present study combines complex cellular co-stimulation with material interaction to successfully replicate key features of glial scar formation, including galectin-3 upregulation and ECM protein accumulation. Further experiments with TGFβ receptor modulators demonstrate promising strategies for reducing glial scarring and offer insights into potential therapeutic interventions for enhancing neuronal regeneration post-CNS injury. Moreover, the study focused on the effects of the interplay between surface energy and surface roughness, highlighting that Pt-sputtered thin film coatings can be highly beneficial in

reducing astrocyte activation. Therefore, this study highlights the importance of in-depth investigations into biomaterial surface properties to advance the development of non-scarring neural implants. Furthermore, it demonstrates how our simplified test platform can complement more complex systems by providing a reproducible and scalable approach to studying biological responses at the cell-material interface.

Author Contributions

Luise Schlotterose: conceptualization, investigation, formal analysis, methodology, visualization, writing original draft; **Duygu Dengiz:** conceptualization, investigation, formal analysis, methodology, visualization, writing original draft; **Eckhard Quandt:** methodology, resources, review; **Karsten Steffens:** methodology; **Dennis Schade:** methodology, review, and editing; **Francois Cossais:** methodology, review, and editing; **Ralph Lucius:** methodology, resources, review, and editing; **Kirsten Hattermann:** conceptualization, investigation, methodology, supervision, resources, review, and editing. All authors read and approved the final manuscript.

Acknowledgments

We thank Judith Becker, Frank Lichte, and Sonja Dahle (Institute of Anatomy, Kiel University) for expert technical assistance and Soeren Kaps (Functional Nanomaterials Group, Kiel University) for his help with the contact angle setup. The artwork was created with BioRender.com. Open Access funding enabled and organized by Projekt DEAL.

Funding

We are grateful for the financial support funded by the German Research Foundation (DFG, RTG2154, materials4brain, P7, P2a and SCHA 1663/6-1). Also, this work was supported by a Newton International Fellowship from the Royal Society.

Conflicts of Interest

The authors declare no conflicts of interest.

Data Availability Statement

The data that support the findings of this study are available from the corresponding author upon reasonable request.

References

1. M. V. Sofroniew, "Molecular Dissection of Reactive Astrogliosis and Glial Scar Formation," *Trends in Neurosciences* 32, no. 12 (2009): 638–647, https://doi.org/10.1016/J.TINS.2009.08.002.

2. V. Bellver-Landete, F. Bretheau, B. Mailhot, et al., "Microglia Are an Essential Component of the Neuroprotective Scar That Forms After Spinal Cord Injury," https://doi.org/10.1038/s41467-019-08446-0.

3. J. E. Burda and M. V. Sofroniew, "Reactive Gliosis and the Multicellular Response to CNS Damage and Disease," *Neuron* 81, no. 2 (2014): 229–248, https://doi.org/10.1016/J.NEURON.2013.12.034.

4. J. W. Fawcett and R. A. Asher, "The Glial Scar and Central Nervous System Repair," *Brain Research Bulletin* 49, no. 6 (1999): 377–391, https://doi.org/10.1016/S0361-9230(99)00072-6.

5. M. Hara, K. Kobayakawa, Y. Ohkawa, et al., "Interaction of Reactive Astrocytes With Type I Collagen Induces Astrocytic Scar Formation Through the Integrin-N-Cadherin Pathway After Spinal Cord Injury," *Nature Medicine* 23, no. 7 (2017): 818–828, https://doi.org/10.1038/NM.4354.

6. J. Kjell, J. Fischer-Sternjak, A. J. Thompson, et al., "Defining the Adult Neural Stem Cell Niche Proteome Identifies Key Regulators of Adult Neurogenesis," *Cell Stem Cell* 26, no. 2 (2020): 277–293.e8, https://doi.org/10.1016/J.STEM.2020.01.002.

7. A. Rolls, R. Shechter, and M. Schwartz, "The Bright Side of the Glial Scar in CNS Repair," *Nature Reviews. Neuroscience* 10, no. 3 (2009): 235–241, https://doi.org/10.1038/nrn2591.

8. M. T. Fitch and J. Silver, "CNS Injury, Glial Scars, and Inflammation: Inhibitory Extracellular Matrices and Regeneration Failure," *Experimental Neurology* 209, no. 2 (2008): 294–301, https://doi.org/10.1016/J.EXPNEUROL.2007.05.014.

9. K. A. Guttenplan, M. K. Weigel, P. Prakash, et al., "Neurotoxic Reactive Astrocytes Induce Cell Death via Saturated Lipids," *Nature* 599, no. 7883 (2021): 102–107, https://doi.org/10.1038/s41586-021-03960-y.

10. J. L. Zamanian, L. Xu, L. C. Foo, et al., "Genomic Analysis of Reactive Astrogliosis," *Journal of Neuroscience* 32, no. 18 (2012): 6391–6410, https://doi.org/10.1523/JNEUROSCI.6221-11.2012.

11. S. A. Liddelow and B. A. Barres, "Reactive Astrocytes: Production, Function, and Therapeutic Potential," *Immunity* 46, no. 6 (2017): 957–967, https://doi.org/10.1016/J.IMMUNI.2017.06.006.

12. S. A. Liddelow, K. A. Guttenplan, L. E. Clarke, et al., "Neurotoxic Reactive Astrocytes Are Induced by Activated Microglia," *Nature* 541, no. 7638 (2017): 481–487, https://doi.org/10.1038/nature21029.

13. B. K. Leung, R. Biran, C. J. Underwood, and P. A. Tresco, "Characterization of Microglial Attachment and Cytokine Release on Biomaterials of Differing Surface Chemistry," *Biomaterials* 29, no. 23 (2008): 3289–3297, https://doi.org/10.1016/J.BIOMATERIALS.2008.03.045.

14. R. Biran, D. C. Martin, and P. A. Tresco, "Neuronal Cell Loss Accompanies the Brain Tissue Response to Chronically Implanted Silicon Microelectrode Arrays," *Experimental Neurology* 195, no. 1 (2005): 115–126, https://doi.org/10.1016/J.EXPNEUROL.2005.04.020.

15. J. Selvakumaran, M. P. Hughes, J. L. Keddie, and D. J. Ewins, "Assessing Biocompatibility of Materials for Implantable Microelectrodes Using Cytotoxicity and Protein Adsorption Studies," 2nd Annual International IEEE-EMBS Special Topic Conference on Microtechnologies in Medicine and Biology. Proceedings (2002), 261–264, https://doi.org/10.1109/MMB.2002.1002326.

16. K. Loger, A. Engel, J. Haupt, et al., "Cell Adhesion on NiTi Thin Film Sputter-Deposited Meshes," *Materials Science and Engineering: C* 59 (2016): 611–616, https://doi.org/10.1016/J.MSEC.2015.10.008.

17. V. A. da Silva, B. C. Bobotis, F. F. Correia, et al., "The Impact of Biomaterial Surface Properties on Engineering Neural Tissue for Spinal Cord Regeneration," *International Journal of Molecular Sciences* 24, no. 17 (2023): 13642, https://doi.org/10.3390/IJMS241713642/S1.

18. W. Yang, Y. Gong, and W. Li, "A Review: Electrode and Packaging Materials for Neurophysiology Recording Implants," *Frontiers in Bioengineering and Biotechnology* 8 (2021): 622923, https://doi.org/10.3389/FBIOE.2020.622923/FULL.

19. S. Kumar Patel, B. Behera, B. Swain, R. Roshan, D. Sahoo, and A. Behera, "A Review on NiTi Alloys for Biomedical Applications and Their Biocompatibility," https://doi.org/10.1016/j.matpr.2020.03.538.

20. M.-A. Crampon, V. Brailovski, M. Sawan, and F. Trochu, "Nerve Cuff Electrode With Shape Memory Alloy Armature: Design and Fabrication," *Bio-Medical Materials and Engineering* 12, no. 4 (2002): 397–410.

21. R. Zhao, X. Liu, Y. Lu, et al., "3D Expandable Microwire Electrode Arrays Made of Programmable Shape Memory Materials," IEEE International Electron Devices Meeting (IEDM), (San Francisco, CA, USA: 2018), https://doi.org/10.1109/IEDM.2018.8614549.

22. D. Dengiz, H. Goldbeck, S. M. Curtis, et al., "Shape Memory Alloy Thin Film Auxetic Structures," *Advanced Materials Technologies* 8, no. 12 (2023): 2201991, https://doi.org/10.1002/ADMT.202201991.

23. P. Velvaluri, A. Soor, P. Plucinsky, R. L. de Miranda, R. D. James, and E. Quandt, "Origami-Inspired Thin-Film Shape Memory Alloy Devices," *Scientific Reports* 11, no. 1 (2021): 1–10, https://doi.org/10.1038/s41598-021-90217-3.

24. C. Chluba, K. Siemsen, C. Bechtold, et al., "Microfabricated Bioelectrodes on Self-Expandable NiTi Thin Film Devices for Implants and Diagnostic Instruments," *Biosensors and Bioelectronics* 153 (2020): 153, https://doi.org/10.1016/J.BIOS.2020.112034.

25. C. Bechtold, R. L. de Miranda, C. Chluba, and E. Quandt, "Fabrication of Self-Expandable NiTi Thin Film Devices With Micro-Electrode Array for Bioelectric Sensing, Stimulation and Ablation," *Biomedical Microdevices* 18, no. 6 (2016): 106, https://doi.org/10.1007/S10544-016-0131-6.

26. M. Gulino, D. Kim, S. Pané, S. D. Santos, and A. P. Pêgo, "Tissue Response to Neural Implants: The Use of Model Systems Toward New Design Solutions of Implantable Microelectrodes," *Frontiers in Neuroscience* 13 (2019): 689, https://doi.org/10.3389/FNINS.2019.00689.

27. E. Redolfi Riva and S. Micera, "Progress and Challenges of Implantable Neural Interfaces Based on Nature-Derived Materials," *Bioelectronic Medicine* 7, no. 1 (2021): 6, https://doi.org/10.1186/S42234-021-00067-7.

28. B. J. Black, M. Ecker, A. Stiller, et al., "In Vitro Compatibility Testing of Thiol-Ene/Acrylate-Based Shape Memory Polymers for Use in Implantable Neural Interfaces," *Journal of Biomedical Materials Research. Part A* 106, no. 11 (2018): 2891–2898, https://doi.org/10.1002/JBM.A.36478.

29. B. A. Koeneman, K. K. Lee, A. Singh, et al., "An Ex Vivo Method for Evaluating the Biocompatibility of Neural Electrodes in Rat Brain Slice Cultures," *Journal of Neuroscience Methods* 137, no. 2 (2004): 257–263, https://doi.org/10.1016/J.JNEUMETH.2004.02.033.

30. L. W. Tien, F. Wu, M. D. Tang-Schomer, E. Yoon, F. G. Omenetto, and D. L. Kaplan, "Silk as a Multifunctional Biomaterial Substrate for Reduced Glial Scarring Around Brain-Penetrating Electrodes," *Advanced Functional Materials* 23, no. 25 (2013): 3185–3193, https://doi.org/10.1002/ADFM.201203716.

31. K. C. Spencer, J. C. Sy, R. Falcón-Banchs, and M. J. Cima, "A Three Dimensional In Vitro Glial Scar Model to Investigate the Local Strain Effects From Micromotion Around Neural Implants," *Lab on a Chip* 17, no. 5 (2017): 795–804, https://doi.org/10.1039/C6LC01411A.

32. V. S. Polikov, E. C. Su, M. A. Ball, J. S. Hong, and W. M. Reichert, "Control Protocol for Robust In Vitro Glial Scar Formation Around Microwires: Essential Roles of BFGF and Serum in Gliosis," *Journal of Neuroscience Methods* 181, no. 2 (2009): 170–177, https://doi.org/10.1016/J.JNEUMETH.2009.05.002.

33. V. S. Polikov, M. L. Block, J. M. Fellous, J. S. Hong, and W. M. Reichert, "In Vitro Model of Glial Scarring Around Neuroelectrodes Chronically Implanted in the CNS," *Biomaterials* 27, no. 31 (2006): 5368–5376, https://doi.org/10.1016/J.BIOMATERIALS.2006.06.018.

34. N. Tasnim, A. Kumar, and B. Joddar, "Attenuation of the In Vitro Neurotoxicity of 316L SS by Graphene Oxide Surface Coating," *Materials Science and Engineering. C, Materials for Biological Applications* 73 (2017): 788–797, https://doi.org/10.1016/J.MSEC.2016.12.123.

35. B. Ghane-Motlagh, M. Sawan, B. Ghane-Motlagh, and M. Sawan, "Design and Implementation Challenges of Microelectrode Arrays: A Review," *Materials Sciences and Applications* 4, no. 8 (2013): 483–495, https://doi.org/10.4236/MSA.2013.48059.

36. F. Amarante dos Santos, "Shape-Memory Alloys as Macrostrain Sensors," *Structural Control and Health Monitoring* 24, no. 1 (2017): e1860, https://doi.org/10.1002/STC.1860.

37. Z. Lifeng, H. Yan, Y. Dayun, et al., "The Underlying Biological Mechanisms of Biocompatibility Differences Between Bare and TiN-Coated NiTi Alloys," *Biomedical Materials* 6, no. 2 (2011): 025012, https://doi.org/10.1088/1748-6041/6/2/025012.

38. T. Habijan, R. L. De Miranda, C. Zamponi, et al., "The Biocompatibility and Mechanical Properties of Cylindrical NiTi Thin Films Produced by Magnetron Sputtering," *Materials Science and Engineering: C* 32, no. 8 (2012): 2523–2528, https://doi.org/10.1016/J.MSEC.2012.07.035.

39. C. Bechtold, R. Lima de Miranda, C. Chluba, C. Zamponi, and E. Quandt, "Method for Fabricating Miniaturized NiTi Self-Expandable Thin Film Devices With Increased Radiopacity," *Shape Memory and Superelasticity* 2, no. 4 (2016): 391–398, https://doi.org/10.1007/S40830-016-0086-8/FIGURES/6.

40. B. Fan, Z. Wei, X. Yao, et al., "Current Advancements in Spinal Cord Injury Research—Glial Scar Formation and Neural Regeneration," *Cells* 12, no. 6 (2023): 853, https://doi.org/10.3390/CELLS12060853.

41. S. Li, X. Gu, and S. Yi, "The Regulatory Effects of Transforming Growth Factor-β on Nerve Regeneration," *Cell Transplantation* 26, no. 3 (2017): 381–394, https://doi.org/10.3727/096368916X693824/ASSET/IMAGES/LARGE/10.3727_096368916X693824-FIG2.JPEG.

42. K. Tzavlaki and A. Moustakas, "TGF-β Signaling," *Biomolecules* 10, no. 3 (2020): 487, https://doi.org/10.3390/BIOM10030487.

43. A. A. Challa, M. Vukmirovic, J. Blackmon, and B. Stefanovic, "Withaferin-A Reduces Type I Collagen Expression In Vitro and Inhibits Development of Myocardial Fibrosis In Vivo," *PLoS One* 7, no. 8 (2012): e42989, https://doi.org/10.1371/JOURNAL.PONE.0042989.

44. S. R. Jeong, M. J. Kwon, H. G. Lee, et al., "Hepatocyte Growth Factor Reduces Astrocytic Scar Formation and Promotes Axonal Growth Beyond Glial Scars After Spinal Cord Injury," *Experimental Neurology* 233, no. 1 (2012): 312–322, https://doi.org/10.1016/J.EXPNEUROL.2011.10.021.

45. F. Hellal, A. Hurtado, J. Ruschel, et al., "Microtubule Stabilization Reduces Scarring and Causes Axon Regeneration After Spinal Cord Injury," *Science* 331, no. 6019 (2011): 928–931, https://doi.org/10.1126/SCIENCE.1201148/SUPPL_FILE/HELLALSOM.PDF.

46. S. Henriksen, G. D. Tylden, A. Dumoulin, B. N. Sharma, H. H. Hirsch, and C. H. Rinaldo, "The Human Fetal Glial Cell Line SVG P12 Contains Infectious BK Polyomavirus," *Journal of Virology* 88, no. 13 (2014): 7556–7568, https://doi.org/10.1128/JVI.00696-14.

47. B. Schweighardt, J. T. Shieh, and W. J. Atwood, "CD4/CXCR4-Independent Infection of Human Astrocytes by a T-Tropic Strain of HIV-1," *Journal of Neurovirology* 7, no. 2 (2001): 155–162, https://doi.org/10.1080/13550280152058816/METRICS.

48. C. Bechtold, R. Lima de Miranda, and E. Quandt, "Capability of Sputtered Micro-Patterned NiTi Thick Films," *Shape Memory and Superelasticity* 1, no. 3 (2015): 286–293, https://doi.org/10.1007/S40830-015-0029-9/FIGURES/8.

49. D. Längle, S. Wojtowicz-Piotrowski, T. Priegann, et al., "Expanding the Chemical Space of Transforming Growth Factor-β (TGFβ) Receptor Type II Degraders With 3,4-Disubstituted Indole Derivatives," *ACS Pharmacology and Translational Science* 7, no. 4 (2024): 1069–1085, https://doi.org/10.1021/ACSPTSCI.3C00371/ASSET/IMAGES/LARGE/PT3C00371_0006.JPEG.

50. J. Schindelin, I. Arganda-Carreras, E. Frise, et al., "Fiji: An Open-Source Platform for Biological-Image Analysis," *Nature Methods* 9, no. 7 (2012): 676–682, https://doi.org/10.1038/NMETH.2019.

51. F. Hejda, P. Solař, and J. Kousal, "Surface Free Energy Determination by Contact Angle Measurements-A Comparison of Various Approaches,".

52. R. J. Good, "Contact Angle, Wetting, and Adhesion: A Critical Review," *Journal of Adhesion Science and Technology* 6, no. 12 (1992): 1269–1302, https://doi.org/10.1163/156856192X00629.

53. T. G. Bush, N. Puvanachandra, C. H. Horner, et al., "Leukocyte Infiltration, Neuronal Degeneration, and Neurite Outgrowth After Ablation of Scar-Forming, Reactive Astrocytes in Adult Transgenic Mice," *Neuron* 23, no. 2 (1999): 297–308, https://doi.org/10.1016/S0896-6273(00)80781-3.

54. E. J. Bradbury and E. R. Burnside, "Moving Beyond the Glial Scar for Spinal Cord Repair," *Nature Communications* 10, no. 1 (2019): 1–15, https://doi.org/10.1038/s41467-019-11707-7.

55. I. Srejovic, D. Selakovic, N. Jovicic, V. Jakovljević, M. L. Lukic, and G. Rosic, "Galectin-3: Roles in Neurodevelopment, Neuroinflammation, and Behavior," *Biomolecules* 10, no. 5 (2020): 798, https://doi.org/10.3390/BIOM10050798.

56. T. N. Ribeiro, L. M. Delgado-García, and M. A. Porcionatto, "Notch1 and Galectin-3 Modulate Cortical Reactive Astrocyte Response After Brain Injury," *Frontiers in Cell and Developmental Biology* 9 (2021): 649854, https://doi.org/10.3389/FCELL.2021.649854/FULL.

57. G. J. Inman, F. J. Nicolás, J. F. Callahan, et al., "SB-431542 Is a Potent and Specific Inhibitor of Transforming Growth Factor-Beta Superfamily Type I Activin Receptor-Like Kinase (ALK) Receptors ALK4, ALK5, and ALK7," *Molecular Pharmacology* 62, no. 1 (2002): 65–74, https://doi.org/10.1124/MOL.62.1.65.

58. D. Längle, T. R. Werner, F. Wesseler, et al., "Toward Second-Generation Cardiomyogenic and Anti-Cardiofibrotic 1,4-Dihydropyridine-Class TGFβ Inhibitors," *ChemMedChem* 14, no. 8 (2019): 810–822, https://doi.org/10.1002/CMDC.201900036.

59. Q. Yuan, Q. Ren, L. Li, et al., "A Klotho-Derived Peptide Protects Against Kidney Fibrosis by Targeting TGF-β Signaling," *Nature Communications* 13, no. 1 (2022): 1–14, https://doi.org/10.1038/s41467-022-28096-z.

60. D. A. G. Mázala, J. S. Novak, M. W. Hogarth, et al., "TGF-β–Driven Muscle Degeneration and Failed Regeneration Underlie Disease Onset in a DMD Mouse Model," *JCI Insight* 5, no. 6 (2020): e135703, https://doi.org/10.1172/JCI.INSIGHT.135703.

61. D. Längle, V. Marquardt, E. Heider, et al., "Design, Synthesis and 3D-QSAR Studies of Novel 1,4-Dihydropyridines as TGFβ/Smad Inhibitors," *European Journal of Medicinal Chemistry* 95 (2015): 249–266, https://doi.org/10.1016/J.EJMECH.2015.03.027.

62. N. J. Laping, E. Grygielko, A. Mathur, et al., "Inhibition of Transforming Growth Factor (TGF)-B1–Induced Extracellular Matrix With a Novel Inhibitor of the TGF-β Type I Receptor Kinase Activity: SB-431542," *Molecular Pharmacology* 62, no. 1 (2002): 58–64, https://doi.org/10.1124/MOL.62.1.58.

63. H. Wang, G. Song, H. Chuang, et al., "Portrait of Glial Scar in Neurological Diseases," *International Journal of Immunopathology and Pharmacology* 31 (2018): 1–6, https://doi.org/10.1177/2058738418801406.

64. M. V. Nastase, M. F. Young, and L. Schaefer, "Biglycan: A Multivalent Proteoglycan Providing Structure and Signals," *Journal of Histochemistry and Cytochemistry* 60, no. 12 (2012): 963–975, https://doi.org/10.1369/0022155412456380.

65. R. E. Baier, "Correlations of Materials Surface Properties With Biological Responses," *Journal of Surface Engineered Materials and Advanced Technology* 5, no. 1 (2015): 42–51, https://doi.org/10.4236/JSEMAT.2015.51005.

66. F. Liu, J. Xu, L. Wu, et al., "The Influence of the Surface Topographical Cues of Biomaterials on Nerve Cells in Peripheral Nerve Regeneration: A Review," *Stem Cells International* 2021 (2021): 8124444, https://doi.org/10.1155/2021/8124444.

67. Y. Shi, R. Liu, L. He, H. Feng, Y. Li, and Z. Li, "Recent Development of Implantable and Flexible Nerve Electrodes," *Smart Materials in Medicine* 1 (2020): 131–147, https://doi.org/10.1016/J.SMAIM.2020.08.002.

68. N. Wu, S. Wan, S. Su, H. Huang, G. Dou, and L. Sun, "Electrode Materials for Brain–Machine Interface: A Review," *InfoMat* 3, no. 11 (2021): 1174–1194, https://doi.org/10.1002/INF2.12234.

69. J. C. Taylor, "Platinum Metallization on Silicon and Silicates," *Journal of Materials Research* 36, no. 1 (2021): 211–234, https://doi.org/10.1557/S43578-020-00084-3.

70. S. N. Bonvicini, B. Fu, A. J. Fulton, Z. Jia, and Y. Shi, "Formation of au, Pt, and Bimetallic au–Pt Nanostructures From Thermal Dewetting of Single-Layer or Bilayer Thin Films," *Nanotechnology* 33, no. 23 (2022): 235604, https://doi.org/10.1088/1361-6528/AC5A83.

71. M. C. Salvadori, L. L. Melo, A. R. Vaz, R. S. Wiederkehr, F. S. Teixeira, and M. Cattani, "Platinum and Gold Thin Films Deposited by Filtered Vacuum Arc: Morphological and Crystallographic Grain Sizes," *Surface and Coatings Technology* 200, no. 9 (2006): 2965–2969, https://doi.org/10.1016/J.SURFCOAT.2004.08.068.

72. S. Metwally and U. Stachewicz, "Surface Potential and Charges Impact on Cell Responses on Biomaterials Interfaces for Medical Applications," *Materials Science and Engineering, C: Materials for Biological Applications* 104 (2019): 109883, https://doi.org/10.1016/J.MSEC.2019.109883.

73. A. D. Gilmour, A. J. Woolley, L. A. Poole-Warren, C. E. Thomson, and R. A. Green, "A Critical Review of Cell Culture Strategies for Modelling Intracortical Brain Implant Material Reactions," *Biomaterials* 91 (2016): 23–43, https://doi.org/10.1016/J.BIOMATERIALS.2016.03.011.

74. H. Chun, J. Lim, K. D. Park, and C. J. Lee, "Inhibition of Monoamine Oxidase B Prevents Reactive Astrogliosis and Scar Formation in Stab Wound Injury Model," *Glia* 70, no. 2 (2022): 354–367, https://doi.org/10.1002/GLIA.24110.

75. D. H. Szarowski, M. D. Andersen, S. Retterer, et al., "Brain Responses to Micro-Machined Silicon Devices," *Brain Research* 983, no. 1–2 (2003): 23–35, https://doi.org/10.1016/S0006-8993(03)03023-3.

76. R. Wang, X. Zhang, J. Zhang, et al., "Oxygen-Glucose Deprivation Induced Glial Scar-Like Change in Astrocytes," *PLoS One* 7, no. 5 (2012): e37574, https://doi.org/10.1371/JOURNAL.PONE.0037574.

77. L. Schlotterose, F. Cossais, R. Lucius, and K. Hattermann, "Resveratrol Alleviates the Early Challenges of Implant-Based Drug Delivery in a Human Glial Cell Model," *International Journal of Molecular Sciences* 25, no. 4 (2024): 2078, https://doi.org/10.3390/IJMS25042078/S1.

78. I. B. Wanner, A. Deik, M. Torres, et al., "A New In Vitro Model of the Glial Scar Inhibits Axon Growth," *Glia* 56, no. 15 (2008): 1691–1709, https://doi.org/10.1002/GLIA.20721.

79. A. K. H. Achyuta, V. S. Polikov, A. J. White, H. G. Pryce Lewis, and S. K. Murthy, "Biocompatibility Assessment of Insulating Silicone Polymer Coatings Using an In Vitro Glial Scar Assay," *Macromolecular Bioscience* 10, no. 8 (2010): 872–880, https://doi.org/10.1002/MABI.200900451.

80. S. Soldozy, S. Young, J. S. Kumar, et al., "A Systematic Review of Endovascular Stent-Electrode Arrays, a Minimally Invasive Approach to Brain-Machine Interfaces," *Neurosurgical Focus* 49, no. 1 (2020): E3, https://doi.org/10.3171/2020.4.FOCUS20186.

81. G. R. John, S. C. Lee, and C. F. Brosnan, "Cytokines: Powerful Regulators of Glial Cell Activation," *Neuroscientist* 9, no. 1 (2003): 10–22, https://doi.org/10.1177/1073858402239587.

82. J. Luo, "TGF-β as a Key Modulator of Astrocyte Reactivity: Disease Relevance and Therapeutic Implications," *Biomedicine* 10, no. 5 (2022): 1206, https://doi.org/10.3390/BIOMEDICINES10051206.

83. G. Song, R. Yang, Q. Zhang, et al., "TGF-β Secretion by M2 Macrophages Induces Glial Scar Formation by Activating Astrocytes In Vitro," *Journal of Molecular Neuroscience* 69, no. 2 (2019): 324–332, https://doi.org/10.1007/S12031-019-01361-5.

84. A. Venkatraman, S. Hardas, N. Patel, N. Singh Bajaj, G. Arora, and P. Arora, "Galectin-3: An Emerging Biomarker in Stroke and Cerebrovascular Diseases," *European Journal of Neurology* 25, no. 2 (2018): 238–246, https://doi.org/10.1111/ENE.13496.

85. W. S. Chen, Z. Cao, H. Leffler, U. J. Nilsson, and N. Panjwani, "Galectin-3 Inhibition by a Small-Molecule Inhibitor Reduces Both Pathological Corneal Neovascularization and Fibrosis," *Investigative Ophthalmology and Visual Science* 58, no. 1 (2017): 9–20, https://doi.org/10.1167/IOVS.16-20009.

86. N. C. Henderson, A. C. Mackinnon, S. L. Farnworth, et al., "Galectin-3 Expression and Secretion Links Macrophages to the Promotion of Renal Fibrosis," *American Journal of Pathology* 172, no. 2 (2008): 288–298, https://doi.org/10.2353/AJPATH.2008.070726.

87. B. T. S. Susarla, E. D. Laing, P. Yu, Y. Katagiri, H. M. Geller, and A. J. Symes, "Smad Proteins Differentially Regulate Transforming Growth Factor-β-Mediated Induction of Chondroitin Sulfate Proteoglycans," *Journal of Neurochemistry* 119, no. 4 (2011): 868–878, https://doi.org/10.1111/J.1471-4159.2011.07470.X.

88. K. Wharton and R. Derynck, "TGFbeta Family Signaling: Novel Insights in Development and Disease," *Development (Cambridge, England)* 136, no. 22 (2009): 3691–3697, https://doi.org/10.1242/DEV.040584.

89. Y. E. Zhang, "Non-Smad Pathways in TGF-β Signaling," *Cell Research* 19, no. 1 (2009): 128–139, https://doi.org/10.1038/cr.2008.328.

90. A. Gunaratne, E. Chan, T. H. El-Chabib, D. Carter, and G. M. Di Guglielmo, "APKC Alters the TGFβ Response in NSCLC Cells Through Both Smad-Dependent and Smad-Independent Pathways," *Journal of Cell Science* 128, no. 3 (2015): 487–498, https://doi.org/10.1242/JCS.155440.

91. A. Gunaratne, B. L. Thai, and G. M. di Guglielmo, "Atypical Protein Kinase C Phosphorylates Par6 and Facilitates Transforming Growth Factor β-Induced Epithelial-To-Mesenchymal Transition," *Molecular and Cellular Biology* 33, no. 5 (2013): 874, https://doi.org/10.1128/MCB.00837-12.

92. Y. Xia, C. Jiang, M. Yang, et al., "SB431542 Alleviates Lupus Nephritis by Regulating B Cells and Inhibiting the TLR9/TGFβ1/PDGFB Signaling," *Journal of Autoimmunity* 132 (2022): 102894, https://doi.org/10.1016/J.JAUT.2022.102894.

93. J. Cao, M. Jiao, Z. Kou, F. Han, and L. Dong, "SB431542 Partially Inhibits High Glucose-Induced EMT by Restoring Mitochondrial Homeostasis in RPE Cells," *Cell Communication and Signaling: CCS* 22, no. 1 (2024): 1–11, https://doi.org/10.1186/S12964-023-01372-1/FIGURES/8.

94. Y. Dong and E. N. Benveniste, "Immune Function of Astrocytes," *Glia* 36, no. 2 (2001): 180–190, https://doi.org/10.1002/GLIA.1107.

95. E. Colombo and C. Farina, "Astrocytes: Key Regulators of Neuroinflammation," *Trends in Immunology* 37, no. 9 (2016): 608–620, https://doi.org/10.1016/J.IT.2016.06.006.

96. L. T. Allen, M. Tosetto, I. S. Miller, et al., "Surface-Induced Changes in Protein Adsorption and Implications for Cellular Phenotypic Responses to Surface Interaction," *Biomaterials* 27, no. 16 (2006): 3096–3108, https://doi.org/10.1016/J.BIOMATERIALS.2006.01.019.

97. M. M. Gentleman and E. Gentleman, "The Role of Surface Free Energy in Osteoblast–Biomaterial Interactions," *International Materials Review* 59, no. 8 (2014): 417–429, https://doi.org/10.1179/1743280414Y.0000000038.

98. A. Wennerberg and T. Albrektsson, "Effects of Titanium Surface Topography on Bone Integration: A Systematic Review," *Clinical Oral Implants Research* 20, no. Suppl 4 (2009): 172–184, https://doi.org/10.1111/J.1600-0501.2009.01775.X.

99. E. Ereifej, "Studying the Glial Cell Response to Biomaterials and Surface Topography for Improving the Neural Electrode Interface," (Wayne State Univ. Diss: 2012).

100. J. Markhoff, M. Krogull, C. Schulze, C. Rotsch, S. Hunger, and R. Bader, "Biocompatibility and Inflammatory Potential of Titanium Alloys Cultivated With Human Osteoblasts, Fibroblasts and Macrophages," *Materials* 10, no. 1 (2017): 52, https://doi.org/10.3390/MA10010052.

101. S. Svensson, M. Forsberg, M. Hulander, et al., "Role of Nanostructured Gold Surfaces on Monocyte Activation and *Staphylococcus Epidermidis* Biofilm Formation," *International Journal of Nanomedicine* 9, no. 1 (2014): 775–794, https://doi.org/10.2147/IJN.S51465.

102. C. P. Pennisi, A. Dolatshahi-Pirouz, M. Foss, et al., "Nanoscale Topography Reduces Fibroblast Growth, Focal Adhesion Size and Migration-Related Gene Expression on Platinum Surfaces," *Colloids and Surfaces. B, Biointerfaces* 85, no. 2 (2011): 189–197, https://doi.org/10.1016/J.COLSURFB.2011.02.028.

103. C. M. Dumont, D. J. Margul, and L. D. Shea, "Tissue Engineering Approaches to Modulate the Inflammatory Milieu Following Spinal Cord Injury," *Cells, Tissues, Organs* 202, no. 1–2 (2016): 52–66, https://doi.org/10.1159/000446646.

104. G. Orive, E. Anitua, J. L. Pedraz, and D. F. Emerich, "Biomaterials for Promoting Brain Protection, Repair and Regeneration," *Nature Reviews. Neuroscience* 10, no. 9 (2009): 682–692, https://doi.org/10.1038/NRN2685.

105. F. Seifried, H. Leiste, R. Schwaiger, S. Ulrich, H. J. Seifert, and M. Stueber, "Structure, Morphology and Selected Mechanical Properties of Magnetron Sputtered (Mo, Ta, Nb) Thin Films on NiTi Shape Memory Alloys. Surf," *Surface and Coatings Technology* 347 (2018): 379–389, https://doi.org/10.1016/J.SURFCOAT.2018.05.014.

106. B. Feng, J. Weng, B. C. Yang, S. X. Qu, and X. D. Zhang, "Characterization of Surface Oxide Films on Titanium and Adhesion of Osteoblast," *Biomaterials* 24, no. 25 (2003): 4663–4670, https://doi.org/10.1016/S0142-9612(03)00366-1.

107. E. S. Ereifej, S. Khan, G. Newaz, J. Zhang, G. W. Auner, and P. J. Vandevord, "Comparative Assessment of Iridium Oxide and Platinum Alloy Wires Using an In Vitro Glial Scar Assay," *Biomedical Microdevices* 15, no. 6 (2013): 917–924, https://doi.org/10.1007/S10544-013-9780-X.

Supporting Information

Additional supporting information can be found online in the Supporting Information section. **Figure S1:** Stress-Strain hysteresis curve of NiTi at 37°C with superelastic behavior up to 4% strain. **Figure S2:** TGFβ-1/2 receptor inhibitors are non-toxic for human SVGA astrocytes in used concentrations. **Figure S3:** Secondary antibody controls. **Figure S4:** Full results from TaqMan Array Human TGFβ Pathway. **Figure S5:** Surface characteristics of insulator layer of SiO_2 (a) SEM image (b) AFM image (c) Contact angle measurements for surface energy, left DMSO and right DI Water results.